Legged Odometry from Body Pose in a Hexapod Robot

Pei-Chun Lin[1], Haldun Komsuoğlu[2], and Daniel E. Koditschek[3]

[1] Department of Mechanical Engineering, The University of Michigan, Ann Arbor, Michigan, USA
pclin@umich.edu
http://www.umich.edu/∼pclin
[2] Department of Electrical Engineering and Computer Science, The University of Michigan, Ann Arbor, Michigan, USA
hkomsuog@umich.edu
http://www.eecs.umich.edu/∼hkomsuog
[3] Department of Electrical Engineering and Computer Science, The University of Michigan, Ann Arbor, Michigan, USA
kod@eecs.umich.edu
http://ai.eecs.umich.edu/people/kod/

Abstract. We report on a continuous time odometry scheme for a walking hexapod robot built upon a previously developed leg-strain based body pose estimator. We implement this estimation procedure and odometry scheme on the robot RHex and evaluate its performance at widely varying speeds and over different ground conditions by means of a 6 degree of freedom vision based ground truth measurement system (GTMS). We also compare the performance to that of sensorless odometry schemes — both legged as well as on a wheeled version of the robot — using GTMS measurements of elapsed distance.

1 Introduction

The hexapod, RHex [1], exhibits unprecedented mobility for a legged autonomous robot [2]. Motivated by the desire to improve dynamical performance of the present open loop controller through the introduction of continuous rigid body state estimates [3], we have recently reported on the development of a novel leg-strain based body pose[1] sensor [4]. Within a stride that maintains at least three non-collinear toes fixed in ground contact, this system delivers a continuous stream of body frame estimates relative to the ground frame at 300 Hz [4]. Additional body proprioceptive sensors — a three degree of freedom (DOF) rate gyro and a six DOF accelerometer array — now under development will lead to the complete 6 DOF continuous time state estimator necessary for advanced feedback control. Notwithstanding this central focus upon sensory feedback control for dynamical gaits, it seems quite interesting to explore along the way the capabilities of the strain based body pose sensor in isolation from these other proprioceptive modalities within quasi-static operational regimes.

[1] We use the term *body pose* to denote the position and orientation of the robot's present body frame relative to the local ground tripod frame within this tripod stance.

In this paper we apply the leg strain based body pose estimator reported in [4] to develop a new sensor that provides complete legged odometry for alternating tripod gaits satisfying the previously stated ground contact conditions: at least three noncollinear toes on the ground at all times. We present a straightforward but general odometry-from-pose algorithm that uses periods of "double support" (where two triads of legs are simultaneously in ground contact) to express the frame of the successor triad in terms of the frame of the predecessor, thereby "remembering" the body's frame relative to the world coordinate system prior to the onset of motion. We stress the system by placing it on increasingly slippery surfaces and report the degradation in performance as a function of surface traction. We compare our sensed odometry scheme to the sensorless alternative of average distance traveled per leg stride[2] as well as to a standard axle revolution count implemented on a wheeled version of the same robot.

The word *odometry*[3] seems to be used in several different contexts in robotics. The traditional notion associated with wheeled vehicles corresponds to planar 3 DOF dead-reckoning by encoder-like sensors that count the rotation of wheels in the absence of other sensors. Here, we generalize this approach to examine the quality of "complete" 6 DOF dead-reckoning for the legged robot — the position and orientation of the robot's present body frame relative to that prior to the initiation of motion.

In reviewing the literature it is similarly useful to distinguish between the positioning problem and the orientation problem. The positioning problem has been treated extensively for wheeled vehicles where the traditional "elapsed distance" measure is combined with body proprioception (accelerometer and gyro data) [5–7] to obtain high quality estimates of the local translation. More recent research is concerned with the fusion of exteroceptive (vision [8], ultrasonic [9], sonar [10], or GPS [11]) sensor data for purposes of obtaining precise global positioning by periodically recalibrating the accumulated dead-reckoning error. In contrast, body orientation estimation has been investigated in the legged robot literature for high-DOF bipeds [12, 13], whose stability and balance must be actively controlled by state feedback. There is some prior work on exteroceptive (vision based) [14–16] approaches to positioning for legged machines but no account of the legged odometry problem. Thus, our treatment of complete 6 DOF odometry appears to be novel.

Section 2 presents the odometry algorithm — a matter of standard geometry and linear algebra involving the position of the presumably known contact-toes in body coordinates. Section 3 examines the accuracy of the resulting odometry estimator implemented on RHex pictured in Figure 1(upper left) using our previously developed leg strain based body pose sensor. We use an independent camera based ground truth measurement system (GTMS) to assess the deterioration in performance over increasingly slippery ground and at varying speeds, as well as to compare the quality of elapsed distance measurements arising from the leg sensor based estimator,

[2] We thank Dr. Johann Borenstein for suggesting this comparison to us.

[3] The Oxford English Dictionary traces the meaning back to its Greek roots *measuring the way*.

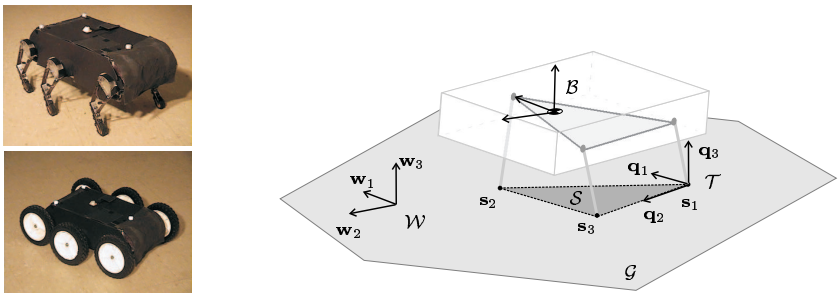

Fig. 1. (Left) RHex and Wheeled RHex; (Right) Sketch illustrating the robot on a flat ground plane, $\mathcal{G}$, within a single stance phase during which it is supported by only three legs whose toes define the support triangle, $\mathcal{S}$. Attached to the support triangle, we define a tripod coordinate system, $\mathcal{T}$.

a legged open loop scheme, and the traditional axle revolution count performed on a wheeled version of RHex pictured in Figure 1(lower left). Section 4 concludes this paper.

2 Computation of Odometry from Body Pose

We develop our odometry algorithm for a hexapod robot in an alternating tripod walking gait because of its utility for RHex. However, the computations below generalize to a family of gaits characterized by two conditions: A) the body is supported by at least three legs with non-collinear toes at any given time; and B) ground contact legs have no toe slippage[4].

In an alternating tripod walking gait we identify two intervals: the *single stance phase* when the body is supported by only one tripod, which denotes the mode of leg contact wherein the three toes of the front and rear ipsilateral legs and the middle contralateral leg of a tripod are all in contact with the ground as depicted in Figure 1(Right); and the *double stance phase* when all legs are in ground contact. This suggests a hierarchically structured algorithm with two levels: 1) a low level, originally presented in [4] and briefly reviewed in Section 2.1, operating during individual single stance phases computing the body pose in a locally defined coordinate system termed tripod coordinate system, $\mathcal{T}$, which is rigidly related to the world coordinate system, $\mathcal{W}$; and 2) a high level sequential composition method relating the tripod coordinate systems in consecutive single stance phases to evaluate the odometry with respect to the world coordinate system, $\mathcal{W}$.

[4] These conditions guarantee that the toe contacts yield a well defined coordinate system fixed in the world frame. Appropriate generalizations of the calculations would extend the computation of odometry to other kinds of legged robots, like quadrupeds or even bipeds with foot (surface) contact.

2.1 Body Pose in Single Stance

It is intuitively clear that knowledge of the configuration relative to the body of each leg in contact with the ground, together with information about the ground contact points yields complete pose information. Assume a "leg model," $\mathbf{s}_i(z_i)$, for each tripod toe, $i = 1, 2, 3$, where z_i denotes the sensory measurements available regarding the configuration of the kinematic chain connecting the robot body to the i$^{\text{th}}$ toe and $\mathbf{s}_i$ represents the point of toe contact with respect to the robot body coordinate system, $\mathcal{B}$. For example, in the RHex implementation, $\mathbf{s}_i(\gamma_i, \sigma_i) = \mathbf{n}_i^{\gamma_i} \circ \mathbf{m}_i(\sigma_i), i = 1, 2, ..., 6$ detailed in [4] consists of the kinematic parameters, γ_i, relating the i$^{\text{th}}$ hip frame, $\mathcal{C}_i$, to the body frame, $\mathcal{B}$, together with the strain across the compliant portion of the leg as read from the sensor suite, σ_i. By defining the tripod coordinate system, $\mathcal{T}$, detailed in [4], whose orthonormal basis $(\mathbf{q}_1, \mathbf{q}_2, \mathbf{q}_3)$ with origin at $\mathbf{s}_1$ is a function of $\mathbf{s}_{i,i=1,2,3}$ as

$$\mathbf{q}_1 := \frac{\mathbf{e}_1 - (\mathbf{q}_2^T \mathbf{e}_1)\mathbf{q}_2}{\left|\left|\mathbf{e}_1 - (\mathbf{q}_2^T \mathbf{e}_1)\mathbf{q}_2\right|\right|_2} \quad \mathbf{q}_2 := \mathbf{e}_2 \quad \mathbf{q}_3 := \mathbf{q}_1 \times \mathbf{q}_2$$

represented in the body coordinate system, $\mathcal{B}$, where $\mathbf{e}_1 := \frac{\mathbf{s}_2 - \mathbf{s}_1}{||\mathbf{s}_2 - \mathbf{s}_1||_2}$ and $\mathbf{e}_2 := \frac{\mathbf{s}_3 - \mathbf{s}_1}{||\mathbf{s}_3 - \mathbf{s}_1||_2}$, we can construct a homogeneous coordinate transformation, $\mathbf{h} : \mathcal{B} \rightarrow \mathcal{T}$, relates the coordinates, $\mathbf{b}$, in body coordinate system, $\mathcal{B}$, to that in the tripod coordinate system, $\mathcal{T}$,

$$\mathbf{h}(\mathbf{b}) := \mathbf{B}\,(\mathbf{b} - \mathbf{s}_1)$$

where $\mathbf{B} := [\mathbf{q}_1\ \mathbf{q}_2\ \mathbf{q}_3]^T$.

2.2 Leg Based Odometry via Composition of Single Stance Measurements

We will now detail how the single stance phase pose computations described above can be integrated over multiple steps to generate this continuous computation of absolute body pose.

First, compute the homogeneous transformation between the tripod coordinate systems of consecutive single stance phases , $\mathcal{T}_j$ and $\mathcal{T}_{j+1}$, as follows. Assuming the toes defining these tripod coordinate systems are stationary (there is no slippage and no liftoff) throughout their presumed stances, and assuming there is an adequate period of double support (the two stance phases overlap for a time sufficient to complete their respective single stance pose computations), both coordinate systems are related to the same (moving) body coordinate system, $\mathcal{B}$. Now, assuming that the prior tripod coordinate system, $\mathcal{T}_j$, has been expressed in world coordinates, the representation of its successor, $\mathcal{T}_{j+1}$, in the world coordinate system follows by the properties of rigid transformations in a straightforward manner that we now detail.

We index single stance phases, $j = 0, 1, ...$, according to their occurrences over the course of locomotion where we denote the j$^{\text{th}}$ single stance tripod coordinate

system by $\mathcal{T}_j$. Without loss of generality, assume that the tripod coordinate system of the first single stance phase coincides with the world coordinate system, $\mathcal{T}_0 \equiv \mathcal{W}$.

The key for establishing the odometry is there exists an intermediate double stance phase where all legs are in ground contact, which allows us to find relationship between tripod coordinate systems of two consecutive single stance phases, $\mathbf{g}_j^{j-1}$: $\mathcal{T}_j \rightarrow \mathcal{T}_{j-1}, \mathbf{g}_j^{j-1} := \mathbf{h}_{j-1} \circ \mathbf{h}_j^{-1}$, before and after this double stance phase. In the on-line implementation where the robot operates on "flat ground," we determine double stance by evaluating a "planarity measure," $\rho(\mathbf{s})$, based upon the sampled covariance matrix of the "sampled toe distribution[5]," $\mathbf{S} = \{\mathbf{s}_1, .., \mathbf{s}_6\}$. The status of double stance is checked if the planarity measure, $\rho(s)$, is dropped under a empirically set threshold, $\overline{\rho}$. When this event is detected we compute the transformations between tripod coordinate systems of consecutive single stance phases, $\mathbf{g}_j^{j-1}$. Figure 2(left) illustrates the flow diagram of the complete on-line algorithm and Figure 2(Right) illustrates the sequential relationship between the tripod coordinate systems, $\mathcal{T}_j$. As a direct consequence, the map, $\mathbf{g}_j^0 : \mathcal{T}_j \rightarrow \mathcal{W}$, relating the j$^{\text{th}}$ tripod coordinate system, $\mathcal{T}_j$, to the world coordinate system, $\mathcal{W} \equiv \mathcal{T}_0$, can be defined recursively,

$$\mathbf{g}_j^0 := \mathbf{g}_{j-1}^0 \circ \mathbf{g}_j^{j-1}, j \in \{1, 2, ...\}$$

where $\mathbf{g}_0^0 := id$. This in turn leads to the definition of the map, $\mathbf{f}_j : \mathcal{B} \rightarrow \mathcal{W}$, that relates the body coordinate system, $\mathcal{B}$, during the j$^{\text{th}}$ single stance phase to the world coordinate system, $\mathcal{W}$, $\mathbf{f}_j := \mathbf{g}_j^0 \circ \mathbf{h}_j$, which is a homogeneous transformation that we prefer to write as

$$\mathbf{f}_j(\mathbf{b}) := \mathbf{A}_j \left(\mathbf{b} - \mathbf{c}_j\right)$$

where $\mathbf{A}_j$ and $\mathbf{c}_j$ denote the rotation matrix and COM translation of the homogeneous transformation accordingly.

The body pose is now read off the entries of the transformation matrices in the familiar manner. The COM is given as

$$\mathbf{r} = [x\, y\, z]^T := -\mathbf{A}_j \mathbf{c}_j$$

and three rotational components of the pose, pitch, α, roll, β, and yaw, γ are computed from the within-stride rotation matrix, $\mathbf{B}_j$ in the standard manner [17] to reduce the possible accumulation error.

[5] Namely, let $\mathbf{P} := \sum_{i=1}^{6} \mathbf{s}_i \mathbf{s}_i^T - \overline{\mathbf{s}}\overline{\mathbf{s}}^T$ where $\overline{\mathbf{s}} := \frac{1}{6}\sum_{i=1}^{6} \mathbf{s}_i$ is the sample mean. Denoting by, $\mathbf{v}$, the eigenvector associated with the smallest eigenvalue of $\mathbf{P}$, we define $\rho(\mathbf{s}) := \frac{1}{6}\sum_{i=1}^{6}[(\mathbf{s}_i - \overline{\mathbf{s}}).\mathbf{v}]^2$ which gives the mean squared distance of the distribution around the best common plane.

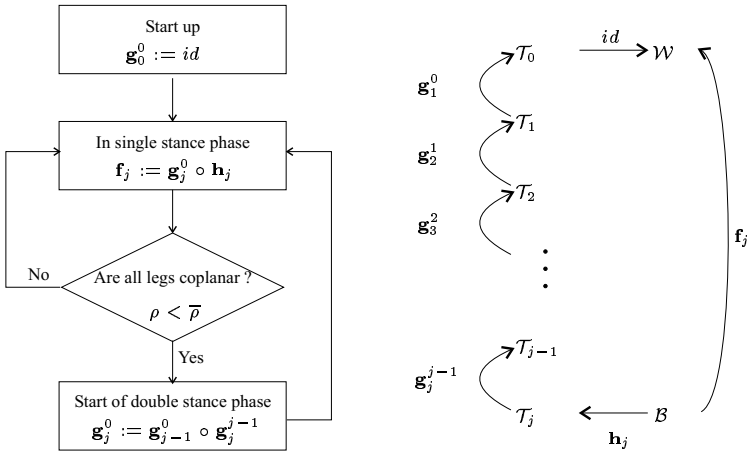

Fig. 2. (Left) Flow chart for the within-stride body pose computation and leg odometry functions; (Right) Commutative diagram relating the tripod coordinate systems, $\mathcal{T}_j$.

3 Performance

We now evaluate the performance of the odometry scheme implemented on RHex in three different scenarios: 1) at varying walking speeds; 2) over dramatically different ground conditions; 3) in comparison to wheeled and sensorless legged versions of the same machine. We report the results using the mean and standard deviation from five runs in each experiment set. The reader should note that RHex's relatively constrained kinematics preclude the exercise of its yaw degree of freedom when it walks with no aerial phase and no toe slippage, hence the implementation we discuss in this section will entail no data of that nature. We compare the estimator output to that of the GTMS (independent visual ground truth measurement system introduced in [4]) with respect to five configuration components — the lateral (x), fore-aft (y), and vertical (z) components of COM translation as well pitch (α) and roll (β) — all in world coordinates, $\mathcal{W}$. Figure 3 plots the comparison for each component over a typical run. We will quantify performance by presenting the standard root mean squared (RMS) error, given by

$$\zeta(d, \hat{d}) := \sqrt{(\left|\left|d - \hat{d}\right|\right|_2^2 / M)}$$

where $d = (d_1, ..., d_M)$ and $d_i := (x_i, y_i, z_i, \alpha_i, \beta_i)$ represents the state trajectory from GTMS; $\hat{d}$ denotes the corresponding state trajectory from output of the algorithm.

Table 1 summarizes the outcome of repeated runs at slow (0.25 m/s), medium (0.35 m/s), and fast (0.51 m/s) speeds, which also includes GTMS measured elapsed distance, ν, and number of tripod strikes for each run, υ, as references. RMS error

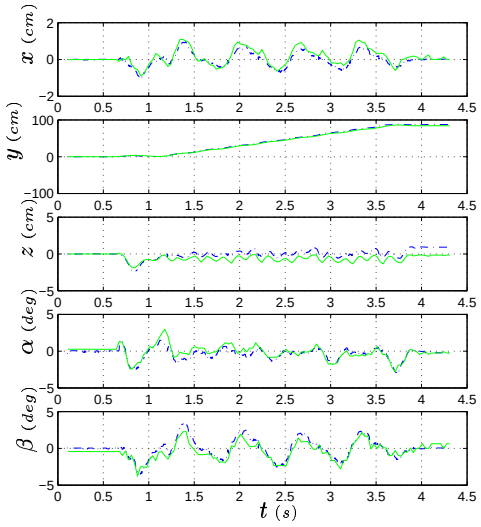

Fig. 3. Odometry measured by GTMS (solid green line) and computed according to our algorithm (dashed blue line).

Table 1. RMS Odometry Error at Varying Walking Speeds (each row representing data averaged over 5 runs with distance, ν and number of strides, υ, shown in reference)

Walking Speed	State					Reference	
	x (cm) avg (std)	y (cm) avg (std)	z (cm) avg (std)	α (deg) avg (std)	β (deg) avg(std)	ν (cm) avg(std)	υ avg(std)
Slow (0.25 m/s)	0.42 (0.13)	4.53 (0.80)	0.30 (0.08)	0.78 (0.09)	0.73 (0.06)	84.0 (6.2)	8.4 (0.5)
Medium (0.35 m/s)	0.41 (0.13)	1.42 (0.32)	0.22 (0.04)	0.60 (0.10)	0.71 (0.08)	83.8 (8.0)	7.8 (0.7)
Fast (0.51 m/s)	0.39 (0.05)	1.41 (0.25)	0.27 (0.04)	0.63 (0.08)	0.68 (0.08)	84.8 (6.5)	7.4 (0.7)

values compared to the robot size (50cm x 25cm x 15cm) indicate successful odometry computation with mean error in angular states less than 1 degree and lateral and vertical positions less than 1 cm. Since slippage during double stance has significant impact on the fore/aft direction of the robot, the corresponding RMS error of y is the largest. We observe that the error in the fore/aft position decreases with increasing speed, attributable to: 1) shorter double stance decreasing the error in the sequential composition computation; and 2) increasing ground reaction forces that decrease slippage.

Table 2 summarizes the outcome of repeated walks at slow speed over four types of surfaces: cardboard ($\mu_s = 0.65$, $\mu_k = 0.60$); plastic ($\mu_s = 0.33$, $\mu_k = 0.27$); plastic with wet soap ($\mu_s = 0.20$, $\mu_k = 0.11$); and plastic with dry soap ($\mu_s = 0.07$, $\mu_k = 0.05$), where the static friction ("stiction") coefficient, μ_s, and kinetic friction coefficients, μ_k, are empirically determined. As these coefficients decrease we observe significant deterioration in computation of linear position in the horizontal plane, (x, y). This is a direct result of the increase in slippage. The angular states,

Table 2. RMS Odometry Error over Different Ground Conditions at slow speed (each row representing data averaged over 5 runs with distance, ν and number of strides, υ, shown in reference)

Ground	State					Reference	
	x (cm) avg (std)	y (cm) avg (std)	z (cm) avg (std)	α (deg) avg (std)	β (deg) avg(std)	ν (cm) avg(std)	υ avg(std)
Cardboard ($\mu_s = 0.65$)	0.42 (0.13)	4.53 (0.80)	0.30 (0.08)	0.78 (0.09)	0.73 (0.06)	84.0 (6.2)	8.4 (0.5)
Plastic ($\mu_s = 0.33$)	0.40 (0.08)	4.45 (0.82)	0.51 (0.05)	0.83 (0.05)	0.65 (0.06)	79.0 (6.2)	8.0 (0.6)
Plastic w/ wetsoap ($\mu_s = 0.20$)	1.39 (0.22)	9.72 (1.30)	0.45 (0.07)	0.63 (0.07)	1.12 (0.22)	73.8 (5.6)	7.4 (0.5)
Plastic w/ drysoap ($\mu_s = 0.07$)	1.82 (0.28)	9.40 (0.56)	0.42 (0.07)	0.63 (0.09)	0.65 (0.05)	78.6 (3.1)	8.2 (0.4)

(α, β), are not affected as severely since they are invariant under the COM translation resulting from uniform leg slippage and their computation only depends on the current single stance phase measurements with no accumulated odometry error. In general, excluding the specially prepared slippery surfaces detailed below, the algorithm performs well and consistently within normal ground conditions characterized by μ_s = 0.33 – 0.65, within which range lie most of the common surfaces when contacted by the rubber toe of robot's leg.

Table 3 compares our leg strain based odometry estimates with sensorless schemes by reference to discrepancies with GTMS measurements of elapsed distance as well as with a wheeled implementation of the Robot pictured in Figure 1(lower left). With no sensing apart from motor shaft measurements, "blind odometry" estimates result from counting the number of leg cycles and multiplying by a previously calibrated "distance-per-cycle" constant. Of course, this is the traditional approach to odometry in wheeled vehicles as well. We ran calibration tests for RHex and a wheeled implementation of the Robot, counting the number of motor shaft cycles over the same long flat "slipless" surface to get the best possible conversion constant. The table presents discrepancies, $\kappa(\%)$ ($=|\Delta\nu|/\nu$), as a percentage of the GTMS measured elapsed distance, ν, for each of the three odometry methods: sensorless legged; pose-based legged; and sensorless wheeled . The results show that the leg strain based odometry from body pose measurements is greatly superior to the blind predictions of the open loop scheme, by nearly an order of magnitude at the higher speeds where the inaccuracies of double support have less effect. The dynamical nature of legged walking (even in the absence of an aerial phase, RHex's gaits exhibit a significant interchange of body kinetic and leg spring potential energy in stance) causes speed variations during locomotion that incur significantly more slippage (exacerbated at slower gaits by prolonged double support) than the far smoother ride afforded by wheels. Thus, our sensor based legged odometry is significantly less accurate than the blind results of counting motor shaft revolutions on the wheeled version of the same machine.

4 Conclusion

We have introduced odometry measurements from a full body pose estimator for a walking hexapod robot based on the kinematic configuration of its legs. We have

Table 3. RHex vs. Wheeled RHex at Varying Speeds and over Different Ground Conditions

	Legged RHex					Wheeled RHex	
	GTMS	sensorless		pose-based		GTMS	
	ν (cm) avg (std)	$\lvert\Delta\nu_d\rvert$ (cm) avg (std)	κ_d (%) avg (std)	$\lvert\Delta\nu_l\rvert$ (cm) avg (std)	κ_l (%) avg (std)	ν_w (cm) avg (std)	κ_w (%) avg (std)
at Varying Speed on Cardboard							
Slow (0.25 m/s)	84.0 (6.2)	17.9 (0.7)	21.4 (2.0)	5.1 (1.9)	6.1 (0.7)	87.6 (3.3)	0.3 (0.09)
Medium (0.35 m/s)	83.8 (8.0)	17.6 (1.8)	21.1 (1.0)	1.8 (0.8)	2.2 (1.0)	83.3 (1.8)	0.3 (0.07)
Fast (0.51 m/s)	84.8 (6.5)	13.9 (3.1)	16.3 (2.9)	1.5 (0.6)	1.7 (0.6)	80.8 (0.9)	0.5 (0.26)
over Different Ground at Slow Speed							
Cardboard	84.0 (6.2)	17.9 (2.2)	21.4 (2.0)	5.1 (1.9)	6.1 (0.7)	87.6 (3.3)	0.3 (0.09)
Plastic	79.0 (6.2)	18.0 (1.9)	22.8 (1.8)	5.3 (3.4)	6.6 (4.4)	87.6 (5.2)	0.3 (0.08)
Plastic w/ wet soap	73.8 (5.6)	16.0 (0.6)	21.8 (1.5)	6.0 (0.4)	8.2 (0.7)	90.2 (4.0)	1.7 (0.22)
Plastic w/ dry soap	78.6 (3.1)	20.9 (2.5)	26.5 (2.9)	14.0 (0.7)	17.8 (0.6)	93.2 (5.1)	1.2 (0.43)

implemented this algorithm on the robot RHex [2] and used a separate visual ground truth measurement system to evaluate the performance at various walking speeds and conditions of surface friction, as well to compare that performance with a wheeled implemented version of the robot. The estimator is shown to perform well at all speeds over normal ground conditions — achieving, for example, mean error in angular states less than 1 degree and lateral and vertical positions less than 1 cm compared to the robot size (50cm x 25cm x 15cm), and five times more accurate legged odometry than computed from averaged open loop distance-per-stride estimates — close to the performance of wheeled vehicles. The estimator continues to function well over a variety of ground conditions, with the onset of significant performance degradation on the most slippery surfaces (soaped plastic) whose coefficient of friction is less than a third that of normal linoleum.

The odometry computation algorithm as described here cannot function if the operating regime includes aerial phases such as those dynamical gaits studied in [18]. To remedy this shortcoming our future work will introduce other sensor modalities such as linear accelerometers and rotational rate gyroscopes to complement the leg kinematic configuration sensor. The more elaborate sensor suite will not only allow us to perform pose estimation during aerial phases but also enable us to detect slippage, the primary source of error in the present scheme, and correct measurements accordingly.

Acknowledgment

The authors would like to thank Prof. R. Brent Gillespie, Prof. Arthur D. Kuo, Dr. Johann Borenstein from University of Michigan, and Prof. Mark R. Cutkosky from Stanford University for their valuable advice. The authors would also like to thank Dr. Gregory C. Sharp for his visual tracking system implementation and Dr. Richard Groff for his suggestions leading to the planarity measure. We would also like to thank Ben Wegbreit from the International Foundation of Robotics Research for the “IFRR Student Fellowship for ISER 2004” to cover the travel expense of P.-C. Lin. This work is supported by DARPA/SPAWAR Contract N66001-00-C-8026 and N66001-03-C-8045.

References

1. M. Buehler, U. Saranli, and D. E. Koditschek, "Single actuator per leg robotic hexapod," U.S. Patent 6,481,513, 2002.
2. U. Saranli, M. Buehler, and D. E. Koditschek, "Rhex - a simple and highly mobile hexapod robot," *International Journal of Robotics Research*, vol. 20, no. 7, pp. 616–631, 2001.
3. U. Saranli and D. E. Koditschek, "Template based control of hexapedal running," in *Proc. IEEE Int. Conf. Robotics and Automation*, vol. 1, 2003, pp. 1374–1379.
4. P.-C. Lin, H. Komsuoglu, and D. E. Koditschek, "A leg configuration sensory system for dynamical body state estimates in a hexapod robot," in *Proc. IEEE Int. Conf. Robotics and Automation*, vol. 1, 2003, pp. 1391–1396.
5. H. H. S. Liu and G. K. H. Pang, "Accelerometer for mobile robot positioning," *IEEE Trans. Industry Application*, vol. 37, no. 3, pp. 812–819, 2001.
6. M. C. Kim and W. K. Chung, "Posture estimation of a car-like mobile robot using disturbance conditions," *Advanced Robotics*, vol. 13, no. 2, pp. 189–202, 1999.
7. H. Chung, L. Ojeda, and J. Borenstein, "Accurate mobile robot dead-rockoning with a precision-calibrated fiber-optic gyroscope," *IEEE Trans. Robot. Automat.*, vol. 17, no. 1, pp. 80–84, 2001.
8. Y. Ma, J. Kosecka, and S. S. Sastry, "Vision guided navigation for a nonholonomic mobile robot," *IEEE Trans. Robot. Automat.*, vol. 15, no. 3, pp. 521–536, Jun 1999.
9. L. Moreno, J. M. Armingol, S. Garrido, A. D. L. Escalera, and M. A. Salichs, "A genetic algorithm for mobile robot localization using ultrasonic sensors," *Journal of Intelligent and Robotic Systems*, vol. 34, no. 2, pp. 135–154, 2002.
10. O. Wijk and H. I. Christensen, "Triangulation-based fusion of sonar data with application in robot pose tracking," *IEEE Trans. Robot. Automat.*, vol. 16, no. 6, pp. 740–752, 2000.
11. P. Goel, S. I. Roumeliotis, and G. S. Sukhatme, "Robust localization using relative and absolute position estimate," in *Proc. IEEE/RSJ Int. Conf. Intelligent Robots and Systems*, vol. 2, 1999, pp. 1134–1140.
12. P. Gorce, "Dynamic postural control method for biped in unknown environment," *IEEE Trans. Robot. Automat.*, vol. 29, no. 6, pp. 616–626, 1999.
13. H. Yoshida, K. Inoue, and Y. Mae, "Mobile manipulation of humanoid robots - optimal posture for generating large force based on statics," in *Proc. IEEE Int. Conf. Robotics and Automation*, vol. 3, 2002, pp. 2271–2276.
14. E. Martinez, "Qualitative vision for the guidance of legged robots in unstructured environments," *Pattern Recognition*, vol. 34, no. 8, pp. 1585–1599, August 2001.
15. G. A. Lopes and D. E. Koditschek, "Visual registration and navigation using planar features," in *Proc. IEEE Int. Conf. Robotics and Automation*, vol. 3, 2003, pp. 3935–3940.
16. K. Hosoda, M. Kamado, and M. Asada, "Vision-based servoing control for legged robots," in *Proc. IEEE Int. Conf. Robotics and Automation*, vol. 4, 1997, pp. 3154–3159.
17. R. P. Paul, *Robot Manipulators - Mathematics, Programming, and Control*. The MIT Press, 1983.
18. U. Saranli, "Dynamic locomotion in a hexapod robot," Ph.D. dissertation, Univerisity of Michigan, August 2002.